Journal of Science and Technology – Smart Systems and Devices
Volume....., Issue....., September 2025, ppp-ppp

Payload Oscillation Mitigation in 3D Tower Cranes via a Model-Free Robust Adaptive Controller

Hue Luu Thi[1,*], Tung Lam Nguyen[2]
[1]*Electric power university*
[2]*Hanoi University of Science and Technology, Hanoi, Vietnam*
[*]*Corresponding author email: huelt@epu.edu.vn*

Abstract
The three-dimensional (3D) tower crane system is a typical underactuated system. Its dynamic model is complex and difficult to determine accurately, while the system operates under harsh environmental conditions. This makes the control problem particularly challenging, as it must simultaneously address both model uncertainties and external disturbances. Inthis paper, a model-free robust adaptive controller is proposed for the three-dimensional tower crane system (3DTC). The controller is designed to suppress (or minimize) payload oscillations while ensuring accurate trajectory tracking under system uncertainties and external disturbances. The proposed approach is developed completely independently of the system model, without relying on any parameter or disturbance estimation mechanism, and it uses only a single time-varying parameter that is updated online. This design strategy results in a simpler controller structure, reducing both the computational burden and design complexity. First, the dynamic model of the 3D tower crane system is formulated to describe the coupling characteristics between the trolley motion and the payload swing. Then, the controller is designed based on this dynamic analysis to achieve robust and adaptive control performance. Lyapunov stability theory is employed to rigorously analyze and guarantee the stability of the closed-loop system. Finally, a series of simulation scenarios are conducted to compare the proposed method with the conventional SMC and the adaptive approach in [1]. This comparison aims to verify its performance and effectiveness under various uncertainties and external disturbances. The results demonstrate that the proposed controller achieves fast convergence, strong robustness, and effective swing suppression, confirming its potential for practical implementation in real-world 3DTC operations.

Keywords: Tower Crane, model-free adaptive controller, underactuated system, unknown parameters of the system.

1. Introduction

The tower crane system is widely used in industry and construction at ports and yards to transport heavy and hazardous loads to desired positions. It is a nonlinear underactuated system, where the number of actuators is fewer than the number of control variables. Furthermore, the non-linear coupling between rotational and translational motion, as well as the dynamics of this system, is highly complex. Therefore, accurately controlling the trolley while simultaneously suppressing load oscillations is a major challenge for the three-dimensional tower crane (3DTC) system. Numerous researchers have proposed various control methods to address this issue, with varying degrees of effectiveness. A sliding mode controller combined with fractional calculus is proposed in [2] to control anti-sway while ensuring that the state variables remain within safe bounds. A novel backstepping control method is developed in [3], which combines the actuated state variables with the underactuated state variables to mitigate payload oscillations as the crane and trolley converge to the desired equilibrium position. In [4], an integral sliding mode control is designed based on a high-fidelity non-linear dynamic model, which reduces model uncertainties. A Lyapunov-based model predictive controller is developed in [5], leveraging the stability conditions of the sliding mode controller to ensure the global stability of the system.

The aforementioned controllers are all designed based on the accuracy of the system model. However, tower crane systems operate in harsh environments and are significantly affected by external disturbances. Additionally, the payload mass changes during operation. To address these issues, several studies have been conducted, such as the sliding mode controller based on disturbance estimation proposed in [6], where disturbance observers are designed to estimate system disturbances for controller input. In [7], a nonlinear disturbance observer is designed to estimate the lumped disturbances. A sliding mode controller is combined with the beneficial effects of the disturbances to suppress payload swing. In [8], a finite-time non-oscillatory sliding mode controller is integrated with a finite-time observer based on the super-twisting algorithm to estimate unknown disturbances. The switching nonlinear logic controller based on a disturbance observer is proposed in [9]. This controller is capable of rapidly suppressing payload oscillation in the presence of complex external disturbances. Furthermore, in [10], an optimal backstepping controller based on a fixed-time

p-ISSN 3093-3285
e-ISSN 3093-3315
https://doi.org/10.51316/jst.192.ssad.2026.36.3.xx
Received: Oct 27, 2025; Revised: Feb 3, 2026;
Accepted: Mar 30, 2026; Online: Jun 3, 2026

disturbance observer is proposed, which compensates for sudden disturbances to minimize their impacton crane operation. The improved non-singular fast terminal sliding mode control in [11] estimates payload mass. In [12, 13], adaptive control methods based on the passivity of 3DTC systems are presented. The adaptive hierarchical sliding mode controller combined with a finite-time disturbance observer is presented in [14] for anti-swing and positioning control of a tower crane system. A novel design using an adaptive output feedback control method with online gravity compensation is proposed in [1], which addresses the disturbance amplification problem caused by the steady-state cable error in tower crane control, as well as accurately estimates the payload. Furthermore, [15] presents a robust adaptive sliding mode controller for a tower crane system, which accurately positions the payload and suppresses oscillation while considering both friction and external wind disturbances. In other research, adaptive input shaping controllers are discussed in [16], [17], where neural networks are used to update the uncertain parameters of the tower crane. A neural network-based adaptive controlleris proposed in [18], which simultaneously addresses uncertain dynamics estimation, uncertain disturbances, and obstacle avoidance. Moreover, fuzzy adaptive control methods employed in [19], [20] demonstrategood control performance even when the system is uncertain and affected by external disturbances.

The adaptive and robust controllers that have been studied address the issues of model uncertainties and external disturbances affecting the system during operation. However, these controllers require the design of observers or estimation tools such as neural networks and fuzzy logic. Consequently, the controllersbecome complex and demand significant computational resources during implementation. This poses challenges to their practical deployment.

This paper proposes a novel model-free robust adaptive controller that does not require the design of observers for disturbance estimation or additional tools for estimating uncertain parameters. This simplification leads to a more straightforward controller design, reduced computational resource requirements, and enhanced potential for practical implementation.

2. Mathematical Model

Figure 1 illustrates the 3DTC's dynamics, whichare modeled using three distinct point masses: the payload mass (m), the trolley mass (M_t), and the equivalent rotational inertia of the crane structure (J_0). The external inputs applied to the system are denoted by the force vector $\mathbf{F} = [\tau_\gamma, f_x, f_l, 0, 0]^T$, where $\tau_\gamma$denotes the torque acting on the rotating base, f_x is the force exerted on the trolley, and f_l corresponds to the tensile force along the hoisting cable. Its state, expressed as $\mathbf{q} = [\gamma, x, l, \varphi, \vartheta]^T$, in which γ is the angular position of the turntable, x represents the trolley's

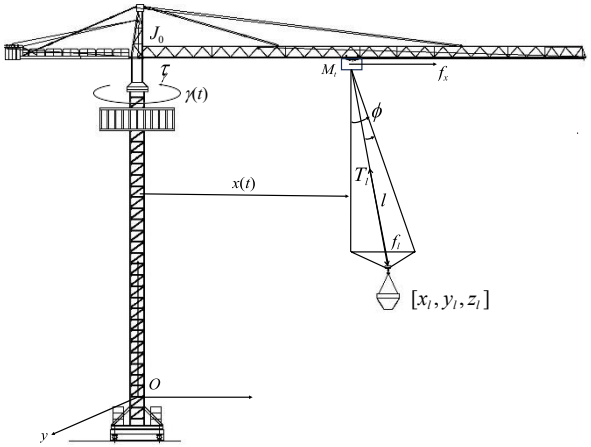

Fig. 1. Model of a three-dimensional tower crane.

horizontal displacement, l denotes the cable length, and φ , ϑ refer to the payload's swing angles in two orthogonal planes. Damping coefficients b_γ , b_x, b_l, b_φ , b_ϑ are introduced to account for frictional forces alongeach particular direction of motion. The coordinates of the payload are given by the position vector $[x_l, y_l, z_l]^T$. The mathematical model of the system is derived using Lagrange's equations and is detailed in [21]. The system dynamics are represented in the following matrix form:

$$\mathbf{M(q)}\ddot{\mathbf{q}} + \mathbf{C(q, \dot{q})}\dot{\mathbf{q}} + \mathbf{G(q)} + \mathbf{D} = \mathbf{F} \quad (1)$$

Equation (1) comprises the following components: a symmetric inertia matrix $\mathbf{M(q)}$; a matrix representing centrifugal and damping effects $\mathbf{C(q, \dot{q})}$; a gravitational term represented by the vector $\mathbf{G(q)}$ and a disturbance vector $\mathbf{D}$ that introduces unknown perturbations into the 3DTC system. The components of the matrices and vectors in (1) can be found in [21].

Assumption 1 *Given that the disturbance* $\mathbf{D}$ *is continuous and bounded, we can find positive numbers* ε_1 *satisfying:* $||\boldsymbol{D}|| \leqslant \varepsilon_1$

Remark 1 *System's parameters and state variables are bounded, implying that the matrix* $\mathbf{M(q)}$, $\mathbf{C(q, \dot{q})\dot{q}}$, *and vector* $\mathbf{G(q)}$ *are also bounded. Consequently, there exists a positive constant* ε_3 *such that* $||\mathbf{M}^{-1}\mathbf{(q)(C(q, \dot{q})\dot{q}} + \mathbf{G(q)}|| \leqslant \varepsilon_3$.

3. Model-free Robust Adaptive Controller

Tower crane systems exemplify underactuated systems due to having more state variables requiring regulation than control inputs. Specifically, the 3DTC system has five state variables, denoted as $\mathbf{q} = [\gamma, x, l, \varphi, \vartheta]^T$, yet there are only three available control inputs $\mathbf{F_a} = [\tau_\gamma , f_x, f_l]^T$. This disparity means that two of the 3DTC's desired outputs are not directly controllable, which inherently poses a control challenge. To facilitate control development, the state vector is partitioned into two subsets: the actuated components $\mathbf{q}_a = [\gamma, x, l]^T$ and

the unactuated components $\mathbf{q}_u = [\phi, \theta]^T$. Accordingly, the dynamic model in (1) is reformulated following this decomposition of the state vector as follows:

$$\mathbf{M}_{aa}(\mathbf{q})\ddot{\mathbf{q}}_a + \mathbf{M}_{au}(\mathbf{q})\ddot{\mathbf{q}}_u + \mathbf{C}_{aa}(\mathbf{q},\dot{\mathbf{q}})\dot{\mathbf{q}}_a + \mathbf{C}_{au}(\mathbf{q},\dot{\mathbf{q}})\dot{\mathbf{q}}_u + \mathbf{G}_{aa}(\mathbf{q}) + \mathbf{D}_{aa} = \mathbf{F_a} \quad (2)$$

$$\mathbf{M}_{ua}(\mathbf{q})\ddot{\mathbf{q}}_a + \mathbf{M}_{uu}(\mathbf{q})\ddot{\mathbf{q}}_u + \mathbf{C}_{ua}(\mathbf{q},\dot{\mathbf{q}})\dot{\mathbf{q}}_a + \mathbf{C}_{uu}(\mathbf{q},\dot{\mathbf{q}})\dot{\mathbf{q}}_u + \mathbf{G}_{uu}(\mathbf{q}) + \mathbf{D}_{uu} = \mathbf{0} \quad (3)$$

where $\mathbf{M}_{aa} \in \Re^{3\times3}$, $\mathbf{M}_{au} \in \Re^{3\times2}$, $\mathbf{C}_{aa} \in \Re^{3\times3}$, $\mathbf{C}_{au} \in \Re^{3\times2}$, $\mathbf{G}_{aa} \in \Re^{3\times1}$, $\mathbf{D}_{aa} \in \Re^{3\times1}$; $\mathbf{M}_{ua} \in \Re^{2\times3}$, $\mathbf{M}_{uu} \in \Re^{2\times2}$, $\mathbf{C}_{ua} \in \Re^{2\times3}$, $\mathbf{C}_{uu} \in \Re^{2\times2}$, $\mathbf{G}_{uu} \in \Re^{2\times1}$, and $\mathbf{D}_{uu} \in \Re^{2\times1}$. Consequently, Equation (3) is rewritten to characterize the unactuated state $\ddot{\mathbf{q}}_u$ as follows:

$$\begin{aligned}\ddot{\mathbf{q}}_u =& -\mathbf{M}_{uu}^{-1}(\mathbf{q})\mathbf{M}_{ua}(\mathbf{q})\ddot{\mathbf{q}}_a - \mathbf{M}_{uu}^{-1}(\mathbf{q})\mathbf{C}_{ua}(\mathbf{q},\dot{\mathbf{q}})\dot{\mathbf{q}}_a \\ & - \mathbf{M}_{uu}^{-1}(\mathbf{q})(\mathbf{C}_{uu}(\mathbf{q},\dot{\mathbf{q}})\dot{\mathbf{q}}_u + \mathbf{G}_{uu}(\mathbf{q}) + \mathbf{D}_{uu})\end{aligned} \quad (4)$$

The substitution of equation (4) into (2) leads to a new expression of the actuation dynamics, which now characterize the actuated state through $\ddot{\mathbf{q}}_a = \mathbf{h}_1(\mathbf{q},\dot{\mathbf{q}})$ as shown below:

$$\begin{aligned}\ddot{\mathbf{q}}_a =& \mathbf{M}_a^{-1}(\mathbf{q})\mathbf{F}_a - \mathbf{M}_a^{-1}(\mathbf{q})\mathbf{C}_a(\mathbf{q},\dot{\mathbf{q}})\dot{\mathbf{q}}_a \\ & - \mathbf{M}_a^{-1}(\mathbf{q})(\mathbf{C}_u(\mathbf{q},\dot{\mathbf{q}})\dot{\mathbf{q}}_u + \mathbf{G}_a(\mathbf{q}) + \mathbf{D}_a)\end{aligned} \quad (5)$$

where:

$$\begin{aligned}&\mathbf{M}_a(\mathbf{q}) = \mathbf{M}_{aa}(\mathbf{q}) - \mathbf{M}_{au}(\mathbf{q})\mathbf{M}_{uu}^{-1}(\mathbf{q})\mathbf{M}_{ua}(\mathbf{q});\\ &\mathbf{C}_a(\mathbf{q},\dot{\mathbf{q}}) = \mathbf{C}_{aa}(\mathbf{q},\dot{\mathbf{q}}) - \mathbf{M}_{au}(\mathbf{q})\mathbf{M}_{uu}^{-1}(\mathbf{q})\mathbf{C}_{ua}(\mathbf{q},\dot{\mathbf{q}});\\ &\mathbf{C}_u(\mathbf{q},\dot{\mathbf{q}}) = \mathbf{C}_{au}(\mathbf{q},\dot{\mathbf{q}}) - \mathbf{M}_{au}(\mathbf{q})\mathbf{M}_{uu}^{-1}(\mathbf{q})\mathbf{C}_{uu}(\mathbf{q},\dot{\mathbf{q}});\\ &\mathbf{G}_a(\mathbf{q}) = \mathbf{G}_{aa}(\mathbf{q}) - \mathbf{M}_{au}(\mathbf{q})\mathbf{M}_{uu}^{-1}(\mathbf{q})\mathbf{G}_{uu}(\mathbf{q}).\\ &\mathbf{D}_a = \mathbf{D}_{aa} - \mathbf{M}_{au}(\mathbf{q})\mathbf{M}_{uu}^{-1}(\mathbf{q})\mathbf{D}_{uu}.\end{aligned}$$

Let us define new variables as follows: $z_1 = \mathbf{q}_u$, $z_2 = \dot{\mathbf{q}}_u$, $z_3 = \mathbf{q}_a$, $z_4 = \dot{\mathbf{q}}_a$, with these substitutions, the original dynamic model of the 3DTC system is re-expressed as:

$$\begin{cases}\dot{z}_1 = & z_2\\ \dot{z}_2 = & \mathbf{f}_2(z_1,z_2,z_3,z_4)\\ \dot{z}_3 = & z_4\\ \dot{z}_4 = & \mathbf{M}_a^{-1}(z_1,z_3)\,\mathbf{F}_a + \mathbf{f}_4(z_1,z_2,z_3,z_4).\end{cases} \quad (6)$$

with $\mathbf{f}_2(z_1,z_2,z_3,z_4) = -\mathbf{M}_{uu}^{-1}(z_1,z_3)(\mathbf{M}_{ua}(z_1,z_3)\dot{z}_4 + \mathbf{C}_{ua}(z_1,z_2,z_3,z_4)z_4 + \mathbf{C}_{uu}(z_1,z_2,z_3,z_4)z_2 + \mathbf{G}_{uu}(z_1,z_3) + \mathbf{D}_{uu})$; $\mathbf{f}_4(z_1,z_2,z_3,z_4) = -\mathbf{M}_a^{-1}(z_1,z_3)(\mathbf{C}_a(z_1,z_2,z_3,z_4)z_4 + \mathbf{C}_u(z_1,z_2,z_3,z_4)z_2 + \mathbf{G}_a(z_1,z_3) + \mathbf{D}_a)$.

The objective of the control problem is to regulate the angular position of the rotary table and the trolley's movement along the reference trajectory toward the desired position, while simultaneously minimizing the swing angle of the payload. The reference swing angle of the payload is $z_{1d} = \mathbf{q}_{ud} = [0,0]^T$; The reference trajectory of the trolley is given by $z_{3d} = \mathbf{q}_{ad} = [\gamma_d, x_d, l_d]^T$. The position and velocity trajectory errors are defined as: $\mathbf{e}_1 = z_1 - z_{1d}$, $\mathbf{e}_3 = z_3 - z_{3d}$ and $\mathbf{e}_2 = z_2 - z_{2d}$, $\mathbf{e}_4 = z_4 - z_{4d}$. As a result, equation (6) can be rewritten in the following form:

$$\begin{cases}\dot{\mathbf{e}}_1 = & \mathbf{I}_{2\times3}\mathbf{M}_a^{-1}(\mathbf{e}_1,\mathbf{e}_3)\mathbf{I}_{3\times2}\,\mathbf{e}_2 + \mathbf{h}_1(\mathbf{e}_1,\mathbf{e}_2,\mathbf{e}_3,\mathbf{e}_4)\\ \dot{\mathbf{e}}_2 = & \mathbf{I}_{2\times3}\mathbf{M}_a^{-1}(\mathbf{e}_1,\mathbf{e}_3)\,\mathbf{e}_3 + \mathbf{h}_2(\mathbf{e}_1,\mathbf{e}_2,\mathbf{e}_3,\mathbf{e}_4)\\ \dot{\mathbf{e}}_3 = & \mathbf{M}_a^{-1}(\mathbf{e}_1,\mathbf{e}_3)\,\mathbf{e}_4 + \mathbf{h}_3(\mathbf{e}_1,\mathbf{e}_2,\mathbf{e}_3,\mathbf{e}_4)\\ \dot{\mathbf{e}}_4 = & \mathbf{M}_a^{-1}(\mathbf{e}_1,\mathbf{e}_3)\,\mathbf{F}_a + \mathbf{h}_4(\mathbf{e}_1,\mathbf{e}_2,\mathbf{e}_3,\mathbf{e}_4).\end{cases} \quad (7)$$

where $\mathbf{I}$ represents an identity matrix, with its size defined according to the index indicated below.

$$\begin{aligned}\mathbf{h}_1(\mathbf{e}_1,\mathbf{e}_2,\mathbf{e}_3,\mathbf{e}_4) =& \big(\mathbf{I}_{2\times2} - \mathbf{I}_{2\times3}\mathbf{M}_a^{-1}(\mathbf{e}_1,\mathbf{e}_3)\mathbf{I}_{3\times2}\big)\mathbf{e}_2;\\ \mathbf{h}_2(\mathbf{e}_1,\mathbf{e}_2,\mathbf{e}_3,\mathbf{e}_4) =& -\mathbf{I}_{2\times3}\mathbf{M}_a^{-1}(\mathbf{e}_1,\mathbf{e}_3)\,\mathbf{e}_3\\ & + \mathbf{f}_2(\mathbf{e}_1,\mathbf{e}_2,\mathbf{e}_3,\mathbf{e}_4)\\ \mathbf{h}_3(\mathbf{e}_1,\mathbf{e}_2,\mathbf{e}_3,\mathbf{e}_4) =& \big(\mathbf{I}_{3\times3} - \mathbf{M}_a^{-1}(\mathbf{e}_1,\mathbf{e}_3)\big)\mathbf{e}_4\\ & - \dot{z}_{3d} + z_{4d}\\ \mathbf{h}_4(\mathbf{e}_1,\mathbf{e}_2,\mathbf{e}_3,\mathbf{e}_4) =& \mathbf{f}_4(\mathbf{e}_1,\mathbf{e}_2,\mathbf{e}_3,\mathbf{e}_4)\end{aligned} \quad (8)$$

Further transformations of variables are introduced as follows:

$$\xi_1 = \frac{\mathbf{e}_1}{W};\ \xi_2 = \frac{\mathbf{e}_2}{W^2};\ \xi_3 = \frac{\mathbf{e}_3}{W^3};\ \xi_4 = \frac{\mathbf{e}_4}{W^4}. \quad (9)$$

$W(t)$ denotes a time-varying coefficient satisfying the initial condition $W(0) = 1$ at $t = 0$, equation (7) is rewritten with the new variables variables $\boldsymbol{\xi}_i$ $(i = 1 \div 4)$ as:

$$\begin{cases}\dot{\xi}_1 = & W\mathbf{I}_{2\times3}\mathbf{M}_a^{-1}(\mathbf{e}_1,\mathbf{e}_3)\mathbf{I}_{3\times2}\xi_2\\ & + \frac{1}{W^1}\mathbf{h}_1(\mathbf{e}) - 1\frac{\dot{W}}{W}\xi_1\\ \dot{\xi}_2 = & W\mathbf{I}_{2\times3}\mathbf{M}_a^{-1}(\mathbf{e}_1,\mathbf{e}_3)\xi_3 + \frac{1}{W^2}\mathbf{h}_2(\mathbf{e})\\ & -2\frac{\dot{W}}{W}\xi_2\\ \dot{\xi}_3 = & W\mathbf{M}_a^{-1}(\mathbf{e}_1,\mathbf{e}_3)\xi_4 + \frac{1}{W^3}\mathbf{h}_3(\mathbf{e})\\ & -3\frac{\dot{W}}{W}\xi_3\\ \dot{\xi}_4 = & \frac{\mathbf{M}_a^{-1}(\mathbf{e}_1,\mathbf{e}_3)}{W^4}\mathbf{F}_a + \frac{1}{W^4}\mathbf{h}_4(\mathbf{e})\\ & -4\frac{\dot{W}}{W}\xi_4\end{cases} \quad (10)$$

where $\mathbf{e} = \left[\mathbf{e}_1^T, \mathbf{e}_2^T, \mathbf{e}_3^T, \mathbf{e}_4^T\right]^T$. The following outlines the control approach developed for the 3DTC system:

$$\mathbf{F}_a = -W^4\boldsymbol{\kappa}_1\mathbf{e}_1 - W^3\boldsymbol{\kappa}_2\mathbf{e}_2 - W^2\boldsymbol{\kappa}_3\mathbf{e}_3 - W\boldsymbol{\kappa}_4\mathbf{e}_4 \quad (11)$$

where $\boldsymbol{\kappa}_i$ are positive definite coefficient matrices, defined as follows: $\boldsymbol{\kappa}_1 = \begin{bmatrix}\kappa_{11} & 0 & 0\\ 0 & \kappa_{12} & 0\end{bmatrix}^T$; $\boldsymbol{\kappa}_2 = \begin{bmatrix}\kappa_{21} & 0 & 0\\ 0 & \kappa_{22} & 0\end{bmatrix}^T$; $\boldsymbol{\kappa}_3 = \mathrm{diag}(\kappa_{31},\kappa_{32},\kappa_{33})$; $\boldsymbol{\kappa}_4 = \mathrm{diag}(\kappa_{41},\kappa_{42},\kappa_{43})$. These coefficient matrices are chosen to ensure that the resulting matrix $\mathbf{A}$ is a Hurwitz matrix. This means that $\mathbf{A}$ satisfies the Lyapunov equation

$\mathbf{A}^T\mathbf{P}+\mathbf{P}\mathbf{A}=-\mathbf{I}_{10\times10}$, where $\mathbf{P}$ is a positive definite symmetric matrix.

$$\mathbf{A}=\begin{bmatrix}\mathbf{0}_{2\times2} & \mathbf{I}_{2\times2} & \mathbf{0}_{2\times3} & \mathbf{0}_{2\times3}\\ \mathbf{0}_{2\times2} & \mathbf{0}_{2\times2} & \mathbf{I}_{2\times3} & \mathbf{0}_{2\times3}\\ \mathbf{0}_{3\times2} & \mathbf{0}_{3\times2} & \mathbf{0}_{3\times3} & \mathbf{I}_{3\times3}\\ -\boldsymbol{\kappa}_1 & -\boldsymbol{\kappa}_2 & -\boldsymbol{\kappa}_3 & -\boldsymbol{\kappa}_4\end{bmatrix} \tag{12}$$

A matrix representation of the differential equations in (10) is obtained as follows:

$$\dot{\boldsymbol{\xi}}=W\mathbf{N}\mathbf{A}\boldsymbol{\xi}+\mathbf{h}(\mathbf{e},W)-\frac{\dot{W}}{W}\boldsymbol{\Omega}\boldsymbol{\xi} \tag{13}$$

where $\boldsymbol{\xi}=\left[\boldsymbol{\xi}_1^T,\boldsymbol{\xi}_2^T,\boldsymbol{\xi}_3^T,\boldsymbol{\xi}_4^T\right]^T$;
$\boldsymbol{\Omega}=\text{diag}(1,1,2,2,3,3,3,4,4,4)$; $\mathbf{e}=[\mathbf{e}_1^T,\mathbf{e}_2^T,\mathbf{e}_3^T,\mathbf{e}_4^T]^T$;
$\mathbf{h}(\mathbf{e},W)=\left[\frac{1}{W^1}\mathbf{h}_1^T(\mathbf{e}),\frac{1}{W^2}\mathbf{h}_2^T(\mathbf{e}),\frac{1}{W^3}\mathbf{h}_3^T(\mathbf{e}),\frac{1}{W^4}\mathbf{h}_4^T(\mathbf{e})\right]^T$

$$\mathbf{N}=\begin{bmatrix}\mathbf{N}_{11} & \mathbf{0}_{2\times2} & \mathbf{0}_{2\times3} & \mathbf{0}_{2\times3}\\ \mathbf{0}_{2\times2} & \mathbf{N}_{22} & \mathbf{0}_{2\times3} & \mathbf{0}_{2\times3}\\ \mathbf{0}_{3\times2} & \mathbf{0}_{3\times2} & \mathbf{M}_a^{-1}(\mathbf{e}_1,\mathbf{e}_3) & \mathbf{0}_{3\times3}\\ \mathbf{0}_{3\times2} & \mathbf{0}_{3\times2} & \mathbf{0}_{3\times3} & \mathbf{M}_a^{-1}(\mathbf{e}_1,\mathbf{e}_3)\end{bmatrix}$$

with $\mathbf{N}_{11}=\mathbf{I}_{2\times3}\mathbf{M}_a^{-1}(\mathbf{e}_1,\mathbf{e}_3)\mathbf{I}_{3\times2}$; $\mathbf{N}_{22}=\mathbf{I}_{2\times3}\mathbf{M}_a^{-1}(\mathbf{e}_1,\mathbf{e}_3)\mathbf{I}_{3\times2}$;
The time-varying parameter is updated according to the following proposed law:

$$\dot{W}=\boldsymbol{\xi}^T\boldsymbol{\xi} \tag{14}$$

Theorem 1 *Consider the system dynamics given in* (1)*, the model-free robust adaptive control input specified in* (11)*, and the adaptive update law for the time-varying parameter defined in* (14)*. Under this framework, both the control error and the states of the closed-loop system asymptotically converge to the origin.*

Proof:
The Lyapunov function is chosen in the form:

$$V=\boldsymbol{\xi}^T\mathbf{P}\boldsymbol{\xi} \tag{15}$$

Differentiating the Lyapunov function (15) and substituting equation (13) yields the following result:

$$\begin{aligned}\dot{V}=&\dot{\boldsymbol{\xi}}^T\mathbf{P}\boldsymbol{\xi}+\boldsymbol{\xi}^T\mathbf{P}\dot{\boldsymbol{\xi}}\\ =&-W\boldsymbol{\xi}^T\mathbf{N}\boldsymbol{\xi}+2\boldsymbol{\xi}^T\mathbf{P}\mathbf{f}(\mathbf{e},W)-2\frac{\dot{W}}{W}\boldsymbol{\xi}^T\mathbf{Q}\boldsymbol{\xi}\end{aligned} \tag{16}$$

where $\mathbf{Q}=\mathbf{P}\boldsymbol{\Omega}$.

Remark 2 *Given that $\dot{W}=\boldsymbol{\xi}^T\boldsymbol{\xi}>0$ and the initial value $W(0)=1$, the function $W(t)$ increases monotonically over time, implying that $W(t)>1$ for all $t>0$. As a result $\frac{-\dot{W}}{W}<0$*

According to Remark 2, the evaluation of the component $-2\frac{\dot{W}}{W}\boldsymbol{\xi}^T\mathbf{Q}\boldsymbol{\xi}$ yields the following:

$$-2\frac{\dot{W}}{W}\boldsymbol{\xi}^T\mathbf{Q}\boldsymbol{\xi}\leqslant-2\frac{\dot{W}}{W}\lambda_{\min}(\mathbf{Q})||\boldsymbol{\xi}||^2\leqslant0 \tag{17}$$

where $\lambda_{\min}(\mathbf{Q})$ is the smallest eigenvalue of $\mathbf{Q}$.

Remark 3 *Based on Assumption 1, Remark 1 and quation* (8)*, there exist positive constants Λ_i such that:* $|\mathbf{h}_i(.)|\leqslant\Lambda_i\sum_{j=1}^{i}|e_j|$ $(j\in N_{1\div4})$.

Based on Remark 3 and equations (8), it is possible to prove that:

$$\begin{aligned}\frac{\mathbf{h}_k}{W^k}&\leqslant\frac{\Lambda_k}{W^k}(|\mathbf{e}_1|+|\mathbf{e}_k|)\quad\text{with }(k=1,2)\\ &\leqslant\Lambda_{\max}(|\boldsymbol{\xi}_1|+|\boldsymbol{\xi}_2|+\mathbf{I}_{2\times3}|\boldsymbol{\xi}_3|+\mathbf{I}_{2\times3}|\boldsymbol{\xi}_4|)\\ &=\Lambda_{\max}[\mathbf{I}_{2\times2},\ \mathbf{I}_{2\times2},\ \mathbf{I}_{2\times3},\ \mathbf{I}_{2\times3}]|\boldsymbol{\xi}|\end{aligned} \tag{18}$$

$$\begin{aligned}\frac{\mathbf{h}_n}{W^n}&\leqslant\frac{\Lambda_n}{W^n}(\mathbf{I}_{3\times2}|\mathbf{e}_1|+\mathbf{I}_{3\times2}|\mathbf{e}_2|+...+|\mathbf{e}_n|)\quad(n=3,4)\\ &\leqslant\Lambda_{\max}(\mathbf{I}_{3\times2}|\boldsymbol{\xi}_1|+\mathbf{I}_{3\times2}|\boldsymbol{\xi}_2|+|\boldsymbol{\xi}_3|+|\boldsymbol{\xi}_4|)\\ &=\Lambda_{\max}[\mathbf{I}_{3\times2},\ \mathbf{I}_{3\times2},\ \mathbf{I}_{3\times3},\ \mathbf{I}_{3\times3}]|\boldsymbol{\xi}|\end{aligned} \tag{19}$$

where $\Lambda_{\max}=\max(\Lambda_1,\Lambda_2,\Lambda_3,\Lambda_4)$, then:

$$\begin{aligned}2\boldsymbol{\xi}^T\mathbf{P}\mathbf{h}(\mathbf{e},W)&\leqslant2|\boldsymbol{\xi}^T||\mathbf{P}||\mathbf{h}(\mathbf{e},W)|\\ &\leqslant2\Lambda_{\max}|\boldsymbol{\xi}^T||\mathbf{P}_c||\mathbf{E}||\boldsymbol{\xi}|\\ &\leqslant8\Lambda_{\max}\lambda_{\max}(\mathbf{P})||\boldsymbol{\xi}||^2\end{aligned} \tag{20}$$

where $\lambda_{\max}(\mathbf{P})$ denotes the largest eigenvalue of the matrix $\mathbf{P}$; $\mathbf{E}=\begin{bmatrix}\mathbf{I}_{2\times2} & \mathbf{I}_{2\times2} & \mathbf{I}_{2\times3} & \mathbf{I}_{2\times3}\\ \mathbf{I}_{2\times2} & \mathbf{I}_{2\times2} & \mathbf{I}_{2\times3} & \mathbf{I}_{2\times3}\\ \mathbf{I}_{3\times2} & \mathbf{I}_{3\times2} & \mathbf{I}_{3\times3} & \mathbf{I}_{3\times3}\\ \mathbf{I}_{3\times2} & \mathbf{I}_{3\times2} & \mathbf{I}_{3\times3} & \mathbf{I}_{3\times3}\end{bmatrix}$.
From (16), (17), and (20), the Lyapunov function's derivative is obtained as follows:

$$\begin{aligned}\dot{V}&\leqslant-W\boldsymbol{\xi}^T\mathbf{B}\boldsymbol{\xi}-2\frac{\dot{W}}{W}\lambda_{\min}(\mathbf{Q}_c)||\boldsymbol{\xi}||^2\\ &+8\Lambda_{\max}\lambda_{\max}(\mathbf{P}_c)||\boldsymbol{\xi}||^2\\ &\leqslant-(W\,N_{\min}-8\Lambda_{\max}\lambda_{\max}(\mathbf{P}))||\boldsymbol{\xi}||^2\\ &-2\frac{\dot{W}}{W}\lambda_{\min}(\mathbf{Q}_c)||\boldsymbol{\xi}||^2.\end{aligned} \tag{21}$$

where $N_{\min}=\min(\mathbf{M}_{aij}^{-1})$.
$W(t)$ is a positive definite parameter satisfying the condition:

$$W(t)\geq\frac{8\Lambda_{\max}\lambda_{\max}(\mathbf{P})+1}{N_{\min}} \tag{22}$$

Therefore

$$\dot{V}\leqslant-\boldsymbol{\xi}^T\boldsymbol{\xi}\leqslant0 \tag{23}$$

From the analysis of (15) and (23), it is established that $\boldsymbol{\xi}$ remains bounded and approaches zero as $t\to\infty$. This implies that all signals of the closed-loop system are bounded, and $W(t)$ is also bounded. Therefore, we have:

$$\lim_{t\to\infty}(\boldsymbol{\xi})=0\quad\text{or}\quad\lim_{t\to\infty}(\mathbf{e})=0 \tag{24}$$

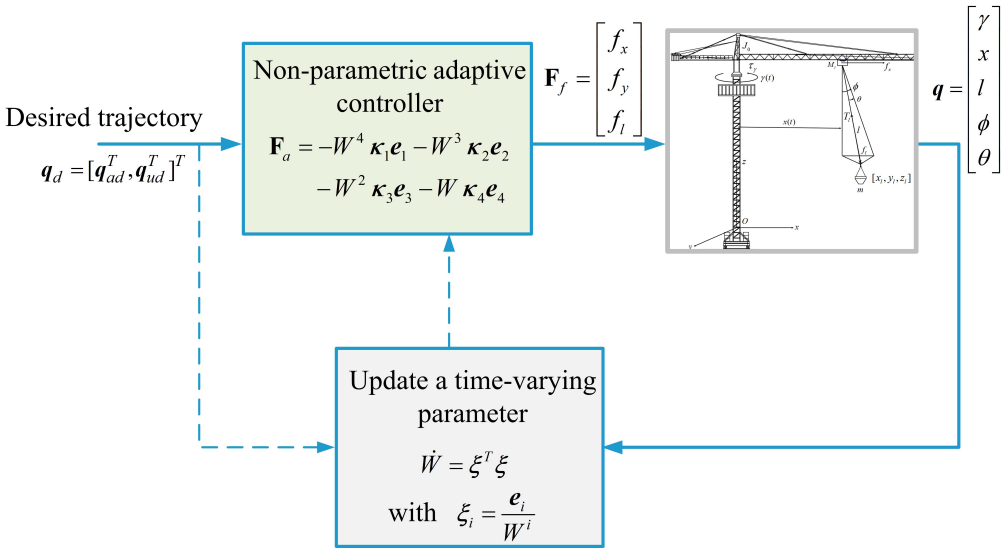

Fig. 2. The control structure of the 3DTC system

The convergence of the control error signals to zero completes the justification of Theorem 1.

As shown in the closed-loop block diagram of Figure 2, the control execution for the 3DTC system is clearly illustrated through the use of a non-parametric robust adaptive controller together with a time-varying parameter estimator.

4. Simulation Results

This section presents the simulation of a 3DTC system, which is regulated by the proposed model-free robust adaptive controller (MFC). The parameters for both the model and the controller are provided [1] as: $m = 0.2$ kg, $J_0 = 6.8$ kg m^2, $M_t = 3$ kg, $b_\gamma = 0.4$Nm/s, $b_x = 0.5$ Nm/s, $b_l = 0.3$ Nm/s, $b_\phi = 0.15$ Nm/s, $b_\theta = 0.15$ Nm/s, $g = 9.81$ m/s^2, $h = 48$m; $\boldsymbol{\kappa}_1 = \mathbf{I}_{3\times 2}$, $\boldsymbol{\kappa}_2 = \mathbf{I}_{3\times 2}$, $\boldsymbol{\kappa}_3$ = diag(200, 400, 200), $\boldsymbol{\kappa}_4$ = diag(10, 100, 20). The initial and final positions of the payload are given as $[\gamma_0, x_0, l_0] = [0, 0, 45]$ (rad,m,m) and $[\gamma_f, x_f, l_f] = [\pi/3, 15, 35]$ (rad,m,m), respectively. The payload is transferred within a time duration of $T = 200$s. The path planning for the payload's movement is outlined below:

$$\begin{cases} \gamma_d = \gamma_0 + \frac{1}{2}(\gamma_f - \gamma_0)(1 - \cos(\frac{\pi t}{T}) \\ x_d = x_0 + (x_f - x_0)\left(3(\frac{t}{T})^3 - 2(\frac{t}{T})^2\right) \text{ with } t \le 200\text{s} \\ l_d = \frac{(l_0 - l_f)}{T^2}(t-T)^2 + l_f \end{cases}$$

$$\begin{cases} \gamma_d = \gamma_f \\ x_d = x_f \\ l_d = \frac{(l_0 - l_f)}{T^2}(t-T)^2 + l_f \end{cases} \quad \text{with } 200s < t \le 400s$$

$$\text{and else } \begin{cases} \gamma_d = \gamma_f \\ x_d = x_f \\ l_d = l_0 \end{cases}$$

Furthermore, comparisons are conducted with two other methods. The controllers under consideration include:

- Controller 1 (C1): The sliding mode control
- Controller 2 (C2): The Adaptive output controller design proposed in [1]
- Controller 3 (C3): The proposed controller.

The C1's proposed control law is defined by:

$$\begin{aligned} \mathbf{F}_a = &-\mathbf{M}_a(\mathbf{q})\Big(2\boldsymbol{\lambda}(\dot{\mathbf{q}}_a - \dot{\mathbf{q}}_{ad}) - \ddot{\mathbf{q}}_{ad} + \boldsymbol{\lambda}^T\boldsymbol{\lambda}(\mathbf{q}_a - \mathbf{q}_{ad}) \\ &+ \boldsymbol{\delta}\dot{\mathbf{q}}_u + \boldsymbol{\lambda}\boldsymbol{\delta}\mathbf{q}_u - \mathbf{K}\text{sign}(\mathbf{s}_0)\Big) \\ &+ \mathbf{C}_a(\mathbf{q}, \dot{\mathbf{q}})\dot{\mathbf{q}}_a + \mathbf{C}_u(\mathbf{q}, \dot{\mathbf{q}})\dot{\mathbf{q}}_u + \mathbf{G}(\mathbf{q}) \end{aligned} \quad (25)$$

where $\mathbf{s}_0$ is the sliding mode surface, which is defined as: $\mathbf{s}_0 = (\dot{\mathbf{q}}_a - \dot{\mathbf{q}}_{ad}) + \boldsymbol{\lambda}(\mathbf{q}_a - \mathbf{q}_{ad}) + \boldsymbol{\delta}\mathbf{q}_u$. The control coefficients are selected as follows: $\mathbf{K} = 0.75\,\text{diag}(0.5, 0.5, 0.5)$; $\boldsymbol{\lambda} = \text{diag}(2, 1.5, 1.5)$; $\boldsymbol{\delta} = \begin{bmatrix} 0.1 & 0 & 0 \\ 0 & 0.4 & 0 \end{bmatrix}^T$.

The C2's structure is described as follows:

$$\tau_\gamma = -k_{p1}\tanh(e_\gamma) - k_{d2}\tanh(s_1 + k_{d1}e_\gamma) + D_\gamma\dot{\gamma} \quad (26)$$

$$f_x = -k_{p2}\tanh(e_x) - k_{d2}\tanh(s_1 + k_{d2}e_x) + D_x\dot{x} \quad (27)$$

$$\begin{aligned} f_l = &-\hat{\Delta} - k_{p3}\tanh(e_l) - k_{d3}\tanh(s_3 + k_{d3}e_l) \\ &- k_s\tanh(e_l)\left(1 - \tanh^2(e_l)\right)\tanh^2(p_1) \\ &- k_s\tanh^2(e_l)\tanh(p_1) + D_l\dot{l} \end{aligned} \quad (28)$$

where $\hat{\Delta}$ represents the estimate of the gravity $\Delta = m_p g$, which can be updated online by: $\dot{\hat{\Delta}} = k\dot{l}$; p is a composite function defined as: $\dot{p}_1 = \dot{e}_l - \lambda_a\tanh(p_1)$; $e_\gamma = \gamma - \gamma_d$; $e_x = x - x_d$ and $e_l = l - l_d$ are positioning errors; s_1, s_2 and s_3 are three auxiliary functions: $\dot{s}_1 = -k_{d1}(s_1 +$

$k_{d1}e_\gamma$); $\dot{s}_2 = -k_{d2}(s_2 + k_{d2}e_x)$; $\dot{s}_3 = -k_{d3}(s_3 + k_{d3}e_l)$. The positive control gains are chosen as follows: $k_{p1} = 500$, $k_{d1} = 45$, $k_{p2} = 250$, $k_{d2} = 32$, $k_{p3} = 250$, $k_{d3} = 20$, $k_s = 0.05$, $\lambda_a = 0.5$, $k = 0.1$

For the simulation, there are two included scenarios:

- Scenario 1. The controller's ability to withstand disturbances is tested by applying harmonic external disturbances to the system.
- Scenario 2. The performance of the controller under parameter changes and stochastic disturbances such as white noise demonstrates its robustness and adaptability.
- Scenario 3. All system parameters undergo significant variations, with values reflecting those of a real-world tower crane system.

4.1. Scenario 1

Simulations are conducted in this section with fixed system parameters, but the system experiences external disturbances defined as follows: $D = [2\sin(100\pi t); 2\sin(105\pi t + \pi/6); 2\sin(85\pi t + 2\pi/3); 2\sin(85\pi t + \pi); 2\sin(85\pi t + \pi/2)]^T$. The results for Scenario 1 are presented in Figures 3 - 4.

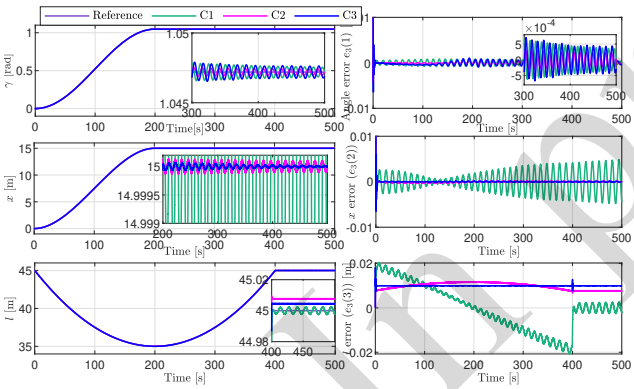

a) The trajectory of the trolley position

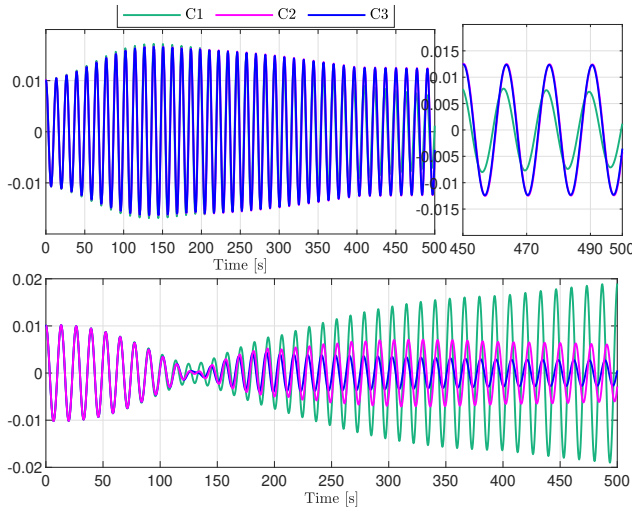

b) Swing angle ϕ and θ.

Fig. 3. Position tracking performances (scenario 1)

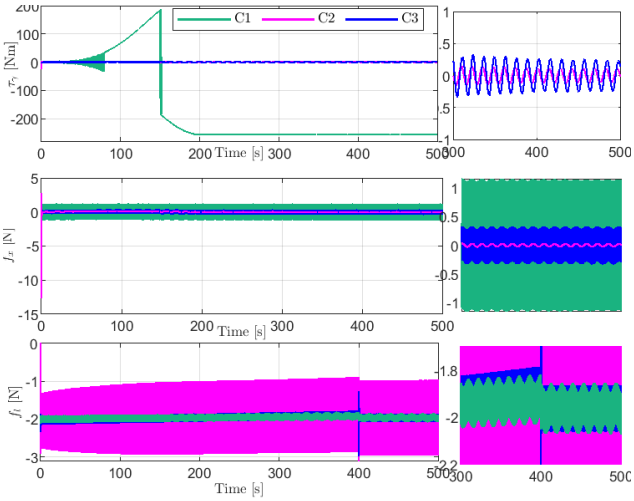

Fig. 4. Force applied to the trolley (scenario 1).

4.2. Scenario 2

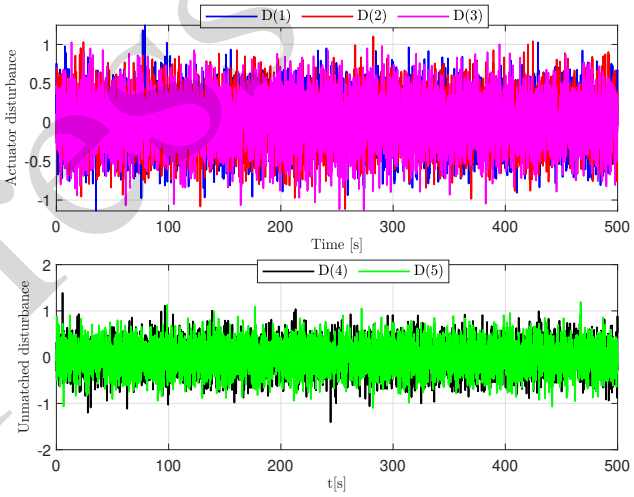

Fig. 5. White noise disturbance.

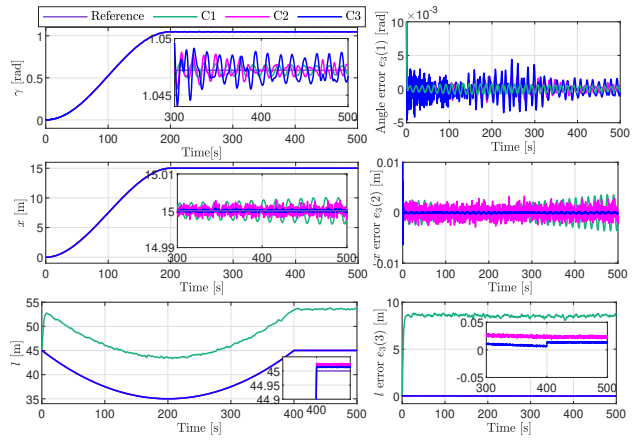

a) The trajectory of the position

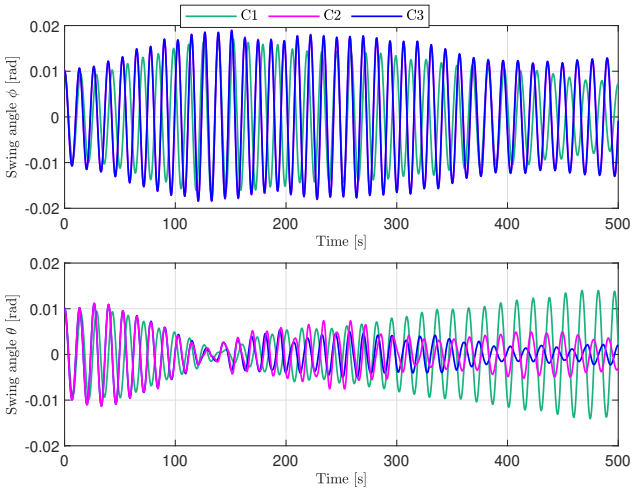

b) Swing angle ϕ and θ.

Fig. 6. Position tracking performances (scenario 2)

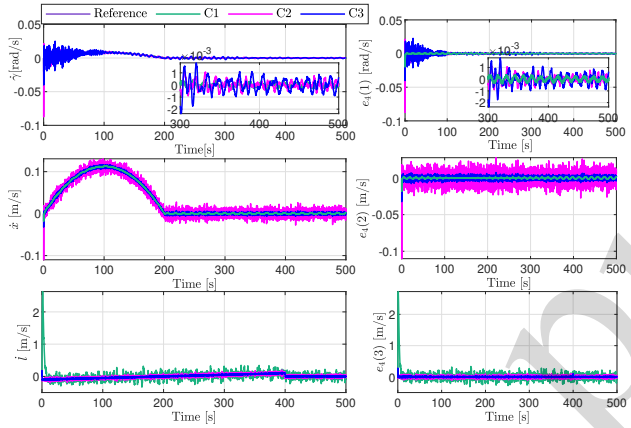

a) The trolley's velocity

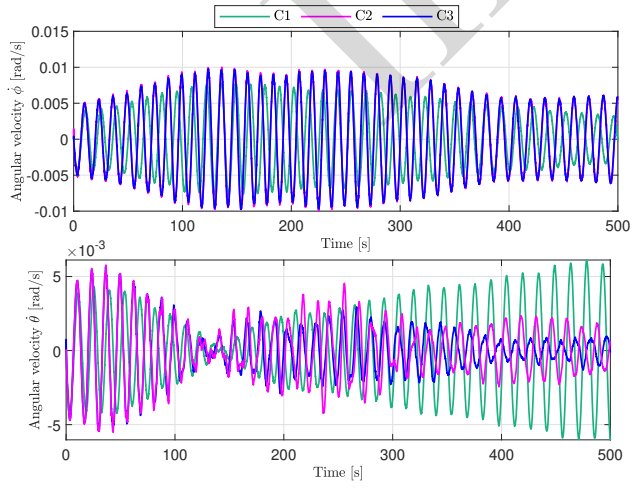

b) The trajectory of angular velocity.

Fig. 7. The payload's velocity (scenario 2)

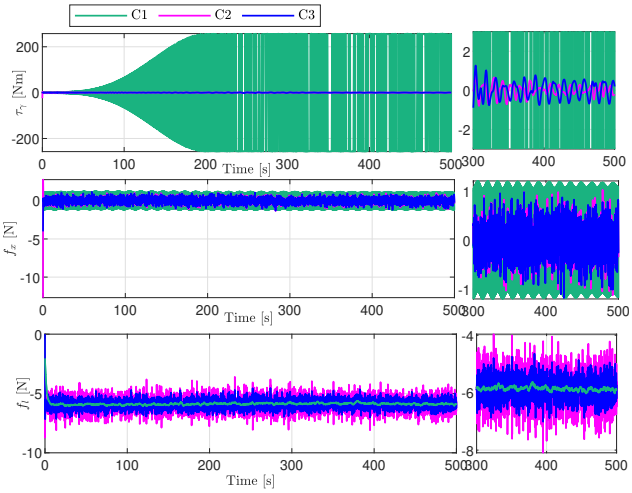

Fig. 8. Force applied to the trolley (scenario 2).

In this case, the mass of the payload is increased to three times its original value, and the system is subjected to a stronger and qualitatively different external disturbance compared to Scenario 1, specifically, white noise, as depicted in Figure 5. The results obtained for Scenario 2 are shown in Figure 6 - Figure 8.

Simulation results from scenario 1 and scenario 2 show that the results demonstrate that both the proposed method and the comparative methods exhibit satisfactory tracking performance, with control errors converging to zero as the payload reaches the equilibrium position. However, the trajectory errors illustrated in Fig. 3a and Fig. 6a indicate that controllers C1 and C2 yield larger errors; furthermore, C1 exhibits a significant steady-state error in the l state. The results in Fig. 3b and Fig. 6b also show that all three controllers achieve effective oscillation suppression, with controller C3 demonstrating a smaller swing angle compared to C1 and C2. As illustrated in Fig. 4 and Fig. 8, the control forces acting on the payload along the axes converge at the equilibrium position. Nevertheless, controller C1 requires a significantly larger control input than controllers C2 and C3.

4.3. Scenario 3

In contrast to the laboratory-scale system in [1], the parameters of a practical tower crane involve much larger values, such as $m = 500$ kg, $M_t = 1140.75$ kg, $b_\gamma = 40$ N·m/s, $b_x = 50$ N·m/s, $b_l = 30$ N·m/s, $b_\phi = 15$ N·m/s, $b_\theta = 15$ N·m/s. The results obtained for Scenario 3 are shown in Figure 9 - Figure 10.

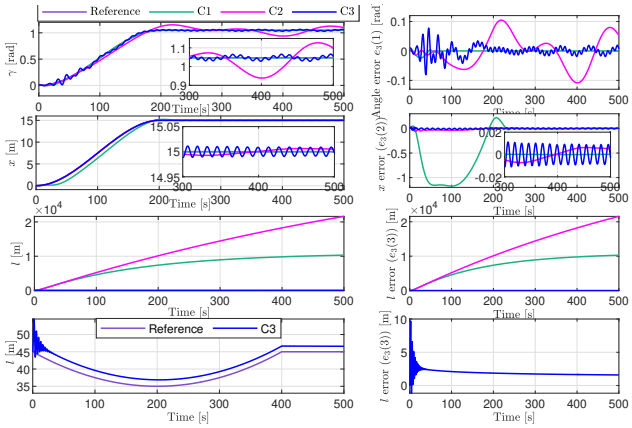

a) The trajectory of the position

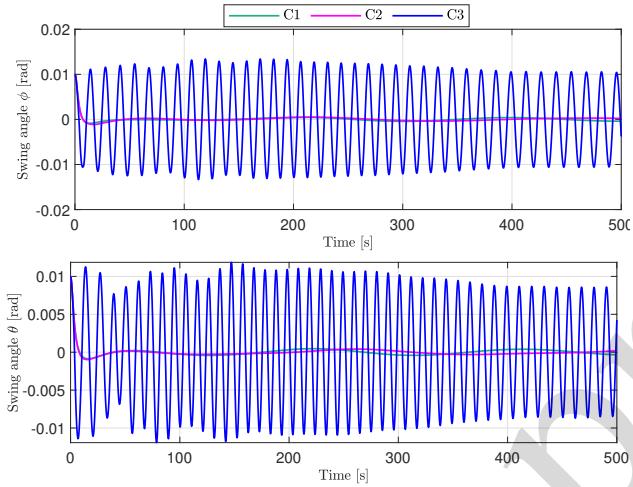

b) Swing angle ϕ and θ.

Fig. 9. Position tracking performances (scenario 3)

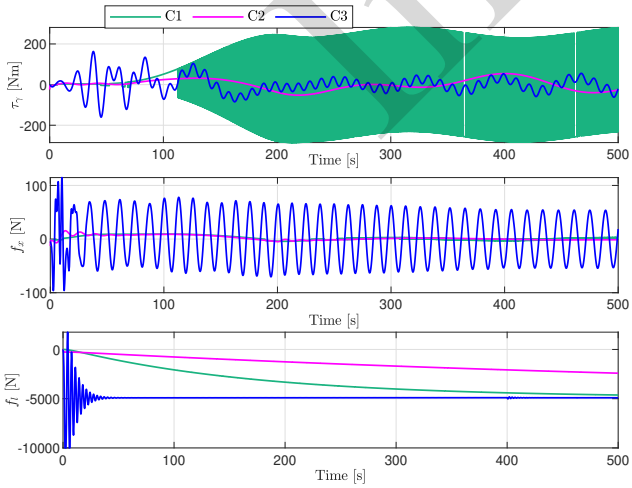

Fig. 10. Force applied to the trolley (scenario 3).

As illustrated in Fig. 9 , the proposed controller (C3) exhibits superior robustness compared to C1 and C2. While the comparative methods fail to manage the heavy payload, resulting in system instability with cable length errors (e_l) diverging to 10^4 m, C3 maintains precise tracking and stability. Specifically, C3 achieves a settling time of 150s and limits swing angles to a negligible 0.01rad despite extreme parameter variations. This confirms that the proposed method is highly resilient, with its performance being minimally affected by fluctuating system parameters. Overall, the simulation results validate that the proposed control scheme ensures high tracking accuracy, superior disturbance rejection, and strong robustness against model uncertainties compared to conventional approaches.

4.4. Discussion

Table 1. Settling Time (s)

Scenario	State	C1	C2	C3
1	γ (rad)	5.15	4.85	**3.15**
	x (m)	∞	120.57	**0.91**
	l (m)	401.25	400.52	**0.27**
2	γ (rad)	6	7.15	**4.85**
	x (m)	∞	∞	**0.90**
	l (m)	∞	∞	**405.27**
3	γ (rad)	3.5	∞	**200.75**
	x (m)	230.5	130.5	**2.5**
	l (m)	N/A	N/A	**57.32**

Table 2. Quantitative Performance Comparison under Various Scenarios

Metric	Scenario	C1	C2	C3
RMSE $[m]$	1	0.008	0.005	0.001
	2	8.5	0.025	**0.002**
	3	Div. (10^4)	Div. (2×10^4)	**2.50**
Max Swing $[rad]$	3	N/A (Failed)	N/A (Failed)	**0.01**
Overshoot (x)	All	Moderate	High	**Negligible**
Control Effort	All	Severe Chattering	Moderate Noise	**Smooth**
Stability	3	Unstable	Unstable	**Stable**

The quantitative data in Tables 1 and 2 highlight the superior performance of the proposed C3 controller across all evaluated scenarios. While C1 and C2 suffer from system instability or divergence in extreme conditions, particularly in Scenario 3, where cable length errors reach magnitudes of 10^4 m, C3 consistently ensures rapid convergence and high tracking precision. Furthermore, C3 demonstrates exceptional robustness by maintaining a negligible swing angle of 0.01 rad and a smooth control signal, effectively eliminating the severe chattering and high energy consumption observed in conventional approaches.

5. Conclusion

In consideration of system uncertainties and external disturbances, this research develops a non-parametric control method to effectively manage the payload trajectory tracking and mitigate its swing angles within a three-dimensional tower crane. We formulate a non-parametric robust adaptive controller that employs a time-varying parameter, thereby minimizing computational burden in hardware implementation and enhancing its practical applicability. Mathematical analysis rigorously substantiates the stability of the

closed-loop system, while simulations demonstrate the efficiency and robustness of the proposed controller. The results demonstrate the effectiveness and robustness of the proposed control strategy, even under significant system uncertainties and external disturbances.

References

[1] M. Zhang, X. Jing, Z. Zhou, and M. Sun, Rapid and restricted swing control via adaptive output feedback for 5-DOF tower crane systems, Mechanical Systems and Signal Processing, vol. 212, Apr. 2024, Art. no. 111283. https://doi.org/10.1016/j.ymssp.2024.111283

[2] T. Zhang, Y. Yang, and J. Li, Fractional-order composite sliding mode control for 4-DOF tower crane systems with given-performance, Automation in Construction, vol. 168, Dec. 2024, Art. no. 105832. https://doi.org/10.1016/j.autcon.2024.105832

[3] N. Li, X. Liu, C. Liu, C. Zhang, H. Wang, and C. Li, Tracking control with enhanced coupling for 5-DOF tower cranes using new block backstepping, Mechanical Systems and Signal Processing, vol. 211, Apr. 2024, Art. no. 111226. https://doi.org/10.1016/j.ymssp.2024.111226

[4] L. T. Aboserre and A. A. El-Badawy, Robust integral sliding mode control of tower cranes, Journal of Vibration and Control, vol. 27, iss. 9-10, pp. 1171–1183, Jun. 2021. https://doi.org/10.1177/1077546320938183

[5] T. H. Luu, V. C. Nguyen, T. L. Nguyen, and Nguyen, Optimal Motion Planning Motivated by Differential Flatness and Lyapunov-Based Model Predictive Control for 5-DOF Tower Cranes, in International Conference on Engineering Research and Applications, 2024, pp. 283–292.

[6] M. Zhang and Jing, Disturbance employment-based sliding mode control for 4-DOF tower crane systems, Mechanical Systems and Signal Processing, vol. 161, pp. 107946, 2021. https://doi.org/10.1016/j.ymssp.2021.107946

[7] C. Zhao, Q. He, J. Zhang, X. Zhu, and Q. Meng, Adaptive sliding mode anti-swing control of 4-DOF tower crane based on a nonlinear disturbance observer, Proceedings of the Institution of Mechanical Engineers, Part C: Journal of Mechanical Engineering Science, vol. 238, no. 21, pp. 10316–10331, 2024. https://doi.org/10.1177/09544062241260710

[8] J. Xia and H. Ouyang, Chattering free sliding-mode controller design for underactuated tower cranes with uncertain disturbance, IEEE Transactions on Industrial Electronics, vol. 71, no. 5, pp. 4963–4975, 2023. https://doi.org/10.1109/TIE.2023.3281665

[9] Y. Qian and Fang, Switching logic-based nonlinear feedback control of offshore ship-mounted tower cranes: A disturbance observer-based approach, IEEE Transactions on Automation Science and Engineering, vol. 16, no. 3, pp. 1125–1136, 2018. https://doi.org/10.1109/TASE.2018.2872621

[10] J. Xia and Ouyang, Fixed-time observer-based back-stepping controller design for tower cranes with mismatched disturbance, Nonlinear Dynamics, vol. 111, no. 1, pp. 355–367, 2023. https://doi.org/10.1007/s11071-022-07851-3

[11] C. Hou and Liu, An improved non-singular fast terminal sliding mode control scheme for 5-DOF tower cranes with the unknown payload masses, frictions and wind disturbances, ISA transactions, vol. 149, pp. 81–93, 2024. https://doi.org/10.1016/j.isatra.2024.04.001

[12] J. Schatz and R. J. Caverly, Payload trajectory tracking of a 5-DOF tower crane with a varying-length hoist cable: A passivity-based adaptive control approach, Mechatronics, vol. 94, pp. 103027, 2023. https://doi.org/10.1016/j.mechatronics.2023.103027

[13] H. Chen and Fang, An adaptive tracking control method with swing suppression for 4-DOF tower crane systems, Mechanical Systems and Signal Processing, vol. 123, pp. 426–442, 2019. https://doi.org/10.1016/j.ymssp.2018.11.018

[14] X. Gu, H. Zhou, M. Hong, S. Ye, and Y. Guo, Adaptive hierarchical sliding mode controller for tower cranes based on finite time disturbance observer, International Journal of Adaptive Control and Signal Processing, vol. 36, no. 9, pp. 2319–2340, 2022. https://doi.org/10.1002/acs.3458

[15] C. Hou, C. Liu, Z. Li, Z. Xin, and H. Zhang, Tower crane systems modeling and adaptive robust sliding mode control design under unknown frictions and wind disturbances, Transactions of the Institute of Measurement and Control, vol. 47, no. 4, pp. 795–809, 2025. https://doi.org/10.1177/0142331224126091

[16] S. F. ur Rehman and Mohamed, Adaptive input shaper for payload swing control of a 5-DOF tower crane with parameter uncertainties and obstacle avoidance, Automation in Construction, vol. 154, pp. 104963, 2023. https://doi.org/10.1016/j.autcon.2023.104963.

[17] S. F. ur Rehman and Mohamed, Input shaping with an adaptive scheme for swing control of an underactuated tower crane under payload hoisting and mass variations, Mechanical Systems and Signal Processing, vol. 175, pp. 109106, 2022. https://doi.org/10.1016/j.ymssp.2022.109106

[18] K. Wang, X. Ma, and J. Li, Neural Network-Based Adaptive Swing Suppression Control for Tower Cranes With Obstacle Avoidance, IEEE/ASME Transactions on Mechatronics, 2024. https://doi.org/10.1109/TMECH.2024.3435794

[19] T.-S. Wu, M. Karkoub, W.-S. Yu, C.-T. Chen, M.-G. Her, and K.-W. Wu, Anti-sway tracking control of tower cranes with delayed uncertainty using a robust adaptive fuzzy control, Fuzzy Sets and Systems, vol. 290, pp. 118–137, 2016. https://doi.org/10.1016/j.fss.2015.01.010

[20] Z. Sun and H. Ouyang, Adaptive fuzzy tracking control for vibration suppression of tower crane with distributed payload mass, Automation in Construction, vol. 142, pp. 104521, 2022. https://doi.org/10.1016/j.autcon.2022.104521

[21] H. L. Thi and T. L. Nguyen, Adaptive finite-time extended state observer-based model predictive control with Flatness motivated trajectory planning for 5-DOF tower cranes, European Journal of Control, vol. 81, pp. 101149, 2025. https://doi.org/10.1016/j.ejcon.2024.101149